ACS APPLIED ENERGY MATERIALS

www.acsaem.org Article

Toward Scalable Perovskite Solar Modules Using Blade Coating and Rapid Thermal Processing

Zhongliang Ouyang, Mengjin Yang, James B. Whitaker, Dawen Li,* and Maikel F. A. M. van Hest*

Cite This: *ACS Appl. Energy Mater.* 2020, 3, 3714−3720 Read Online

ACCESS | Metrics & More | Article Recommendations | Supporting Information

ABSTRACT: Toward scalable manufacturing of perovskite solar panels, high-performance planar p−i−n perovskite solar cells (PVSCs) and modules have been demonstrated with blade coating and rapid thermal processing (RTP). The PVSCs made using RTP for less than 30 s have equivalent photovoltaic performance as devices fabricated from hot-plate annealing for 2 min. The resulting PVSCs show the best average power conversion efficiency (PCE) of over 18.47% from forward and reverse scans. Mini-modules with an active area of over 2.7 cm^2 exhibit a champion average PCE of over 17.73% without apparent hysteresis. To the best of our knowledge, these efficiencies are the highest for PVSCs processed by the combination of blade coating and RTP. Furthermore, both the blade coating and RTP were performed in an ambient environment, paving the way for the large-scale production of PVSCs through high-speed roll-to-roll printing.

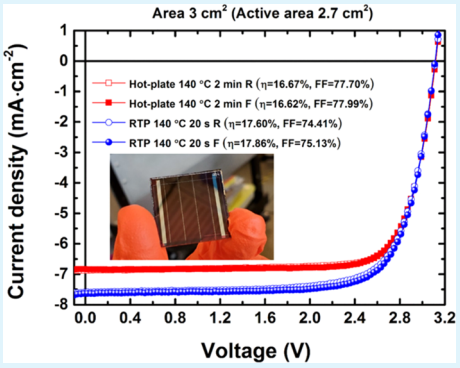

KEYWORDS: *rapid thermal processing, blade coating, large area, mini-modules, perovskite solar cells*

1. INTRODUCTION

The power conversion efficiency (PCE) of perovskite solar cells (PVSCs) has rapidly increased from 3.8% to more than 25.2% in the past decade.[1−4] So far, all of the PVSCs that broke the world record of efficiency have an active area smaller than 0.1 cm^2. Small active areas are commonly adopted worldwide in scientific demonstration and technology development for one reason: it is much simpler to maintain the uniformity of the coated films across a small area and therefore much easier to achieve better efficiency. Small active area can only be used for the demonstration of performance possibilities, but beyond that, it has no practical use. There are two main factors that limit the upscaling of PVSCs. One is the coating technique and the other is the annealing process. The most prevalent methods for coating and annealing are spin coating and convective thermal annealing (i.e., hot plate), respectively. These approaches are dependable but could never easily be scaled up to module size areas. Advanced coating and annealing practices should be adopted to obtain uniform and good quality films on large areas.

Among scalable printing technologies, blade coating has been demonstrated to be successful in perovskite photovoltaics.[5−7] Blade coating provides advantages such as the capability of processing a wide range of fluids with high and low viscosities.[8] Moreover, blade coating is a great step up from spin coating toward ultimate roll-to-roll (R2R) deposition with slot-die coating.[9,10] In addition, blade coating is more suitable in the lab scale compared to the slot-die coating because the former will not have to deal with the dead volume like the latter and thus it will consume less ink in small batches.[11] To realize large-scale manufacturing of PVSCs, traditional annealing methods like hot-plate annealing should be avoided since they are energy-inefficient and time-consuming (at a time scale of minutes or an hour), which will impede the high-speed character of blade coating or any other R2R printing technique.[12−22] Nevertheless, annealing processes other than hot-plate annealing continue to be explored. Microwave radiation was utilized to anneal mixed-halide perovskites $CH_3NH_3PbI_{3-x}Cl_x$. Xu et al. showed an annealing time of 6 min resulting in devices with a PCE of only 10.29%.[23] Wang et al. demonstrated postannealing microwave treatment also on $CH_3NH_3PbI_{3-x}Cl_x$ and improved the efficiency to 13.39%.[24] Three minutes of microwave irradiation was cast on $CH_3NH_3PbI_3$ ($MAPbI_3$) perovskite films to fabricate PVSCs with PCEs of up to 14.91%.[25] In addition to the low efficiencies, the microwave annealing is likely not compatible with the R2R printing since it requires a closed environment to confine the microwave energy. Near-infrared (NIR) laser was used to crystallize $MAPbI_3$ perovskite films, leading to a device PCE of 11.3%.[26] A 450 nm laser was adopted to anneal $MAPbI_3$ perovskite films, resulting in an optimal efficiency of 17.8%.[27] Laser annealing was claimed to

Received: January 27, 2020
Accepted: April 1, 2020
Published: April 1, 2020

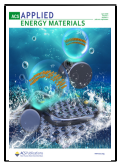

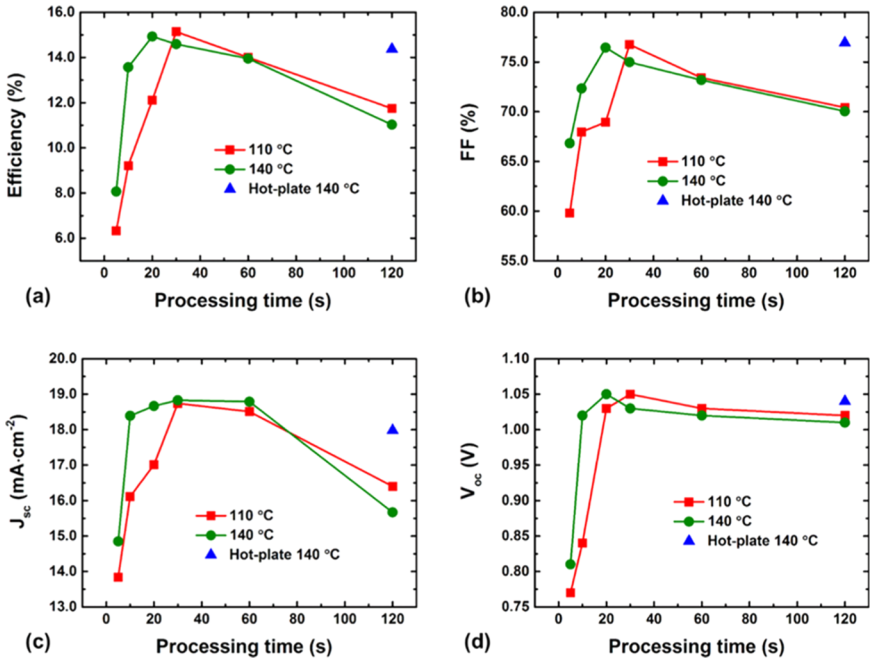

Figure 1. Trends of (a) efficiency, (b) FF, (c) J_{sc}, and (d) V_{oc} at different RTP temperatures for different times. Active area = 0.105 cm^2.

achieve faster crystallization of perovskite films than the thermal annealing, but it is difficult to be scaled up due to slow raster scan rate, thereby small area coverage. Flash lamp annealing was demonstrated on $MAPbI_3$ perovskite films with an annealing time of less than 3 ms by using a high-energy xenon light. In terms of X-ray diffraction (XRD) results, this flash xenon light produced films with better crystallinity than the conventional thermal annealing, but no device was made.[28] Also with a xenon lamp, Troughton et al. demonstrated a PCE of 11.3% by flash-annealing $CH_3NH_3PbI_{3-x}Cl_x$ perovskite films in 1 ms.[29] Lavery et al. pulse-annealed $MAPbI_3$ thin films within 2 ms via intense light irradiated from a xenon lamp. The consequential devices exhibited PCEs of up to 12.3%, which is similar to those of their thermally annealed samples.[30] With the help of intense pulsed xenon light and diiodomethane additive, Ankireddy et al. were able to fabricate $MAPbI_3$-based PVSCs with a device efficiency of 16.5%.[31] Compared with the above-mentioned photonic annealing methods, rapid thermal processing (RTP, also known as rapid thermal annealing, RTA) is a widely used technique in the industry for processing semiconductors.[32] Sanchez et al. applied RTP annealing to inorganic mixed-halide $CsPbI_xBr_{3-x}$ perovskite films, achieving a PCE of over 10%.[33] With 40 s of RTP, Pool et al. attained a PCE of 14.15% on inorgainc formamidinium lead iodide ($FAPbI_3$) perovskite films, comparable to the efficiency of 13.80% from hot-plate annealing.[34] Park et al. annealed mixed-cation $(MAPbI_3)_{0.85}(FAPbI_3)_{0.15}$ perovskite layer by RTP at 120 °C for 10 min under a N_2 atmosphere. Their device PCE surpassed 17% but was accompanied by a low fill factor (FF) of 68%.[35] With 3 min of RTP in nitrogen, Dou et al. managed to make $MAPbI_3$-based PVSCs with a PCE of 18.0%.[36] All of the aforementioned researches employed small device area (0.1 cm^2 or smaller); it was not until recently that larger device area has been implemented with radiative annealing. RTP annealing has been shown to work on both the $MAPbI_3$ and triple-cation mixed-halide (MAFACsPbIBr) perovskite layers, producing PVSCs with an active area of 1.4 cm^2. The corresponding PCEs have been reported to reach 14.6% with an FF of 69.8% and ∼15.0% with an FF of ∼61%, respectively.[37,38] Compared with their small devices, both the efficiency and FF dropped considerably. Although RTP appeared functioning on perovskite films, none of the aforesaid investigations went beyond spin coating for the deposition of the perovskite active layer. So far, only Breuning et al. combined the blade coating with RTP to manufacture PVSCs in helium. Their champion device displayed a PCE of 16.8% with an active area of 0.1 cm^2.[39]

In this study, blade coating and RTP have been used to fabricate planar p−i−n PVSCs and modules. The PVSCs made from RTP for less than 30 s have equivalent photovoltaic performance as devices fabricated from hot-plate annealing for 2 min. The RTP method successfully decreases the annealing time of blade-coated $MAPbI_3$ films by more than 4-fold as compared to the conventional thermal annealing. The resulting small devices with an active area of 0.105 cm^2 show the best average PCE of over 18.47% from forward and reverse scans. Mini-modules with an active area of over 2.7 cm^2 exhibit a champion average PCE of over 17.73% from forward and reverse scans. To the best of our knowledge, these efficiencies are the highest for PVSCs processed by the combination of blade coating and RTP. Furthermore, high fill factors have been achieved, with average values of 79.90 and 74.77% for the small device and mini-module, respectively. In addition, both the blade coating and RTP were performed in an ambient environment. These results justify the feasibility of RTP for the upscaling fabrication of PVSCs. Although blade coating has been proven to be effective in the lab scale, more advanced deposition methods such as slot-die coating are required to team up with RTP to realize R2R printing and large-scale production of PVSCs.

2. RESULTS

2.1. Thermal Budget of RTP on the Perovskite Layer. The annealing effect of RTP on the PCE of PVSCs was investigated methodically. To explore the thermal budget of RTP, planar p−i−n PVSCs with a structure of indium tin oxide (ITO)/poly(triaryl amine) (PTAA)/poly[(9,9-bis(3′-(*N*,*N*-

https://dx.doi.org/10.1021/acsaem.0c00180
ACS Appl. Energy Mater. 2020, 3, 3714−3720

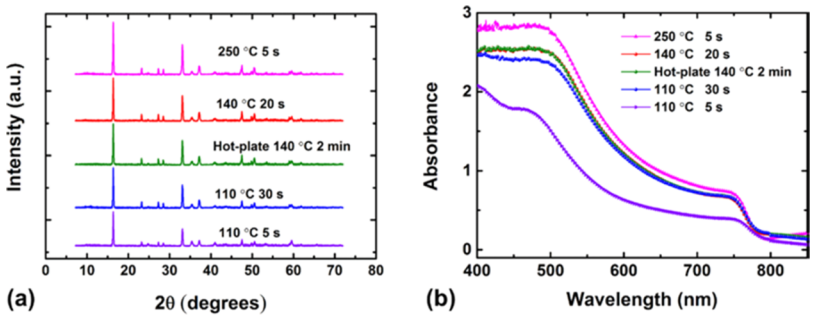

Figure 2. (a) XRD and (b) UV−vis results of selected annealing conditions.

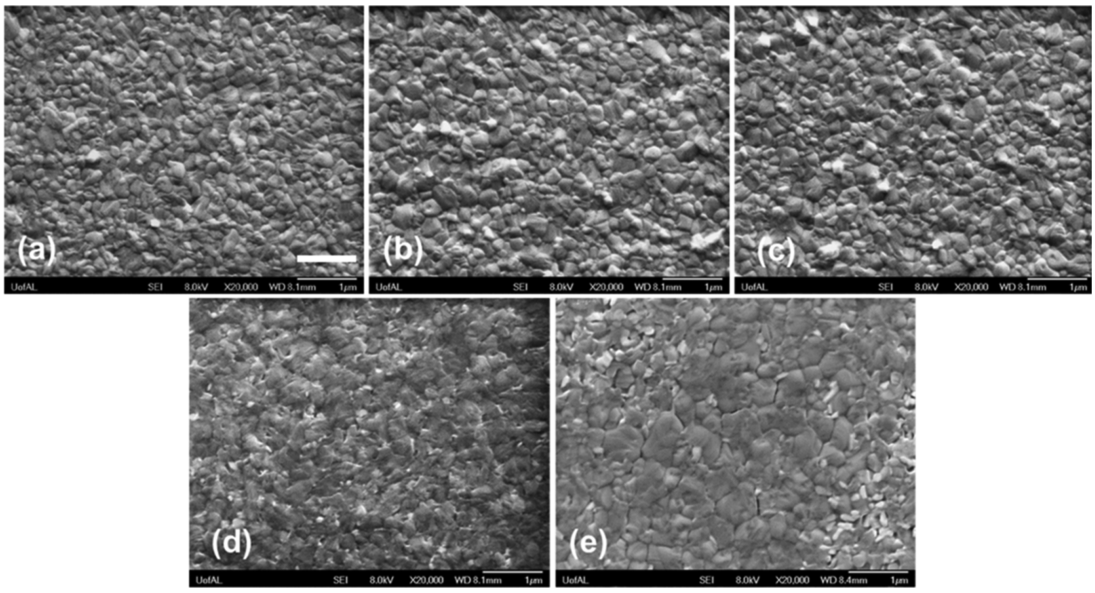

Figure 3. Top-view SEM images of RTP films at (a) 110 °C for 30 s, (b) 140 °C for 20 s, (c) hot-plate-annealed at 140 °C for 2 min, (d) 110 °C 5 s, and (e) 250 °C 5 s. The scale bar is 1 μm.

dimethylamino)propyl)-2,7-fluorene)-*alt*-2,7-(9,9-dioctylfluorene)] (PFN)/$MAPbI_3$/C_{60}/bathocuproine (BCP)/Ag were fabricated. Figure 1 shows the trends of photovoltaic parameters of PVSCs based on both hot-plate-annealed $MAPbI_3$ films and RTP-annealed $MAPbI_3$ films with different RTP temperatures and time. The photovoltaic parameters have been extracted directly from J−V characteristics, including PCE, fill factor (FF), short-circuit current density (J_{SC}), and open-circuit voltage (V_{OC}). The detailed photovoltaic values are summarized in Table S1. The reference PVSC contains the $MAPbI_3$ layer hot-plate-annealed at 140 °C for 2 min (120 s). In contrast, the trends of RTP at 110 and 140 °C are included in Figure 1 for side-by-side comparison with the hot-plate annealing. It can be seen that regardless of temperature, there are PCE peaks for RTP as a function of the annealing time. For RTP at 110 °C, the highest PCE occurs at 30 s of annealing time, with a value of 15.14%. One the other hand, 20 s of annealing appears the best for RTP at 140 °C, with a PCE of 14.93%. The FFs, J_{SC}, and V_{OC} follow the same trend as that of PCEs for both RTP temperatures, drastically changing in the range between 5 and 120 s. With a fixed RTP temperature, the variation of RTP time is equal to the changing of energy supply to crystallization and formation of perovskite films. A time scale of 120 s might not be overwhelming for hot-plate annealing but is certainly too long in the case of RTP. Thus, it is not hard to understand the observed substantial effects of RTP temperatures and time on photovoltaic performance. Unlike the PCE and FF, both J_{SC} and V_{OC} see trends with obvious plateaus, especially with V_{OC}, between 30 and 120 s. A PVSC is first a diode; once the diode is formed, the voltage response is not expected to change radically. For both RTP temperatures in Figure 1, the annealing time of 5 or 10 s is not sufficient to form high-quality perovskite films that are good enough for devices. On the contrary, the annealing time of over 60 s is apparently more than the perovskite films can handle, resulting in considerable degradation on the device performance. More trends are plotted in Figure S1 using the data from Table S1, with fixed RTP time (5, 10, and 20 s) but varying RTP temperature. With decreasing RTP time, it is clear that elevated temperatures are needed for the peak PCEs, from 140 °C at 20 s to 200 °C at 5 s. In general, it is the energy rather than the temperature or time alone that determines the annealing process. Energy amount less than necessary is not able to completely anneal perovskite films. An excessive amount of energy will degrade perovskite films, and energy overdose will eventually create films that have poor quality and show inferior performance. This is why there are optimized temperatures and associated heating times for different perovskite layers in different publications. Although the product of temperature and time has no corresponding physical term, it is a good indication of the total energy provided. With a fixed temperature, the variation of time is

https://dx.doi.org/10.1021/acsaem.0c00180
ACS Appl. Energy Mater. 2020, 3, 3714−3720

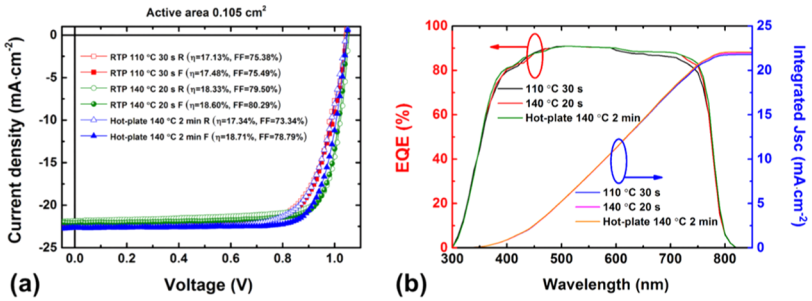

Figure 4. (a) $J-V$ curves of RTP devices at 110 °C for 30 s and 140 °C for 20 s, and hot-plate-annealed at 140 °C for 2 min. (b) EQEs of the corresponding devices.

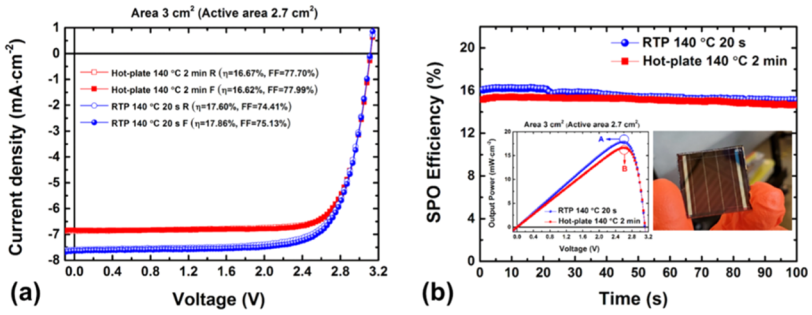

Figure 5. (a) $J-V$ curves of mini-modules made from RTP at 140 °C for 20 s and hot-plate-annealed at 140 °C for 2 min. (b) Quasi-SPOs of the corresponding mini-modules. Active area = 2.7 cm^2. Inset left: $P-V$ curves of mini-modules; Inset right: photograph of a mini-module.

equal to the changing of energy supply to crystallization and formation of perovskite films. A better way is to use the energy flux and time to calculate the energy supplied.[40] Simply speaking, increasing the temperature is to increase the energy flux. In terms of hot-plate and RTP annealing, controlling the temperature and time is relatively easy, while it is impossible to determine the corresponding energy flux and total energy that is delivered to the target film. As a result, there is a proper temperature range that can be used to avoid energy overdose on the target film for thermal annealing, including hot-plate and RTP annealing. The highlighted (dashed line) section in Table S1 outlines those RTP conditions that can over-anneal $MAPbI_3$ films, i.e., turn film color to yellow, indicating decomposing of $MAPbI_3$ into PbI_2. The hot-plate control PVSC shows a PCE of 14.37%, an FF of 76.93%, a J_{SC} of 17.98 mA/cm^2, and a V_{OC} of 1.04 V. The RTP-treated samples achieved similar PCE, FF, J_{SC}, and V_{OC} at two specific conditions: 110 °C for 30 s and 140 °C for 20 s. It is worth noting that these temperatures of RTP are set-point temperatures, and the actual temperature might not be the same, especially the perovskite films. The entire annealing process happens within tens of seconds; it is impossible to measure the actual temperature of the perovskite films in the current experimental setup (more details in the Section 4.2 Device Fabrication).

Figure 2 shows X-ray diffraction (XRD) spectra and UV−visible (UV−vis) absorbance of samples from selected annealing conditions. XRD and UV−vis results are very close for three conditions: RTP at 110 °C for 30 s, RTP at 140 °C for 20 s, and hot-plate annealing at 140 °C for 2 min. This is in good agreement with the similar photovoltaic performance shared by these three annealing conditions. The sample annealed by RTP at 110 °C for 5 s has sharp but weakest peak intensity. It means that the $MAPbI_3$ has formed but not reached a good quality yet, supported by its much weaker UV−vis absorbance than those from other annealing conditions. Figure 3 compares scanning electron microscopy (SEM) top-view morphologies of $MAPbI_3$ films from selected annealing conditions. Similar densely packed films with defined grains have been observed for the same three conditions: RTP at 110 °C for 30 s, RTP at 140 °C for 20 s, and hot-plate annealing at 140 °C for 2 min. The SEM image of a disordered morphology verifies that RTP at 110 °C for 5 s provides insufficient energy for annealing the perovskite film. In contrast, RTP at 250 °C for 5 s supplies an overdose of energy to the perovskite film, leading to larger grain sizes, which might explain the higher UV−vis absorbance and XRD peak intensity, but also damaging the film and creating cracks and possibly other defects in it.

More devices have been made on the best RTP conditions, as well as the hot-plate control condition. Figure 4a shows a comparison between our best hot-plate reference device and top RTP devices. The device from hot-plate annealing demonstrates PCEs of 17.34 and 18.71% from forward and reverse scans, respectively. PVSCs with RTP at 140 °C for 20 s yield a slightly overall better photovoltaic performance, with PCEs of 18.33 and 18.60% from forward and reverse scans, respectively. In contrast, RTP at 110 °C for 30 s leads to PCEs slightly less than 17.5%. Figure 4b exhibits the external quantum efficiency (EQE) and the corresponding integrated J_{SC} of the devices with the same annealing conditions, as shown in Figure 4a. RTP at 140 °C for 20 s and hot-plate annealing at 140 °C for 2 min have almost identical EQE curve, marginally better than that of RTP at 110 °C for 30 s. In spite of annealing methods, the integrated J_{SC}s calculated from the EQEs are very close to the values acquired from $J-V$ measurements (Figure 4a). The good match between $J-V$ and EQE measurements confirms the validity of obtained photovoltaic parameters. The similarities of photovoltaic performance from RTP at 140 °C for 20 s and hot-plate

https://dx.doi.org/10.1021/acsaem.0c00180
ACS Appl. Energy Mater. 2020, 3, 3714−3720

annealing at 140 °C for 2 min also agree with the findings from XRD, UV−vis and SEM results. Nevertheless, the demonstrated RTP devices showed comparable photovoltaic performance to their hot-plate-annealed counterparts, underlining the success of such a radiative treatment for building high-performance PVSCs. More importantly, the annealing time of RTP is significantly shorter than that of the traditional thermal annealing (20 s versus 2 min). As a result, RTP has much better compatibility with large-scale manufacturing methods such as R2R processing. Assuming an R2R printing speed of 10 cm/s,[41] the RTP equipment will only need 2 m length (10 cm/s times 20 s) as compared to a 12 m long (10 cm/s times 2 min) oven if the traditional thermal annealing is used.

2.2. Upscaling of PVSCs. Mini-modules of PVSCs have been made, adopting the optimal RTP condition, i.e., 140 °C for 20 s and the hot-plate condition 140 °C for 2 min. The detailed structure of mini-modules can be found in previous works.[42] Each mini-module comprises three subcells monolithically interconnected in series. The designated area of a mini-module is 3 cm^2 (including the dead area from interconnections) with a geometric fill factor of 0.9, giving an active device area of 2.7 cm^2. Figure 5 shows a comparison between the champion RTP mini-module and the best hot-plate-annealed mini-module. In Figure 5a, $J-V$ curves of RTP mini-module exhibit an active area PCE of over 17.73%, which is comparable to the active area PCE of over 16.65% from the hot-plate-annealed mini-module. The difference in PCEs is mainly from different J_{SC} and FF. The RTP and hot-plate mini-modules have an almost identical V_{OC} = 3.12 V, which is equivalent to an average of 1.04 V for each individual subcell for these three-cell mini-modules. The photovoltaic performance of the RTP mini-module is very similar to that of the small area device, as shown in Figure 4a. This not only confirms that the RTP/blade-coated perovskite film has high quality over the large area but also proves that the combination of RTP and blade coating is suitable for upscaling the manufacture of PVSCs. Figure 5b provides quasi-SPO (stabilized power output) of the RTP and hot-plate mini-modules. The quasi-SPO has been measured with an approximating method by sweeping voltage in a very small range near the maximal power point (MPP) for some time. The left inset of Figure 5b marks the respective MPPs (points A and B) for the RTP and hot-plate mini-modules in their power−voltage ($P-V$) curves. The right inset of Figure 5b is a photograph of the mini-module. The statistics of the $J-V$ measurements is displayed in Figure S2. The data for the box charts were extracted from over 30 $J-V$ measurements for RTP and hot-plate mini-modules each. It is worth noting that all of the measurements, $J-V$ and quasi-SPO, were carried out in an ambient environment without any thermal or humidity control. In addition, the quasi-SPOs were measured after all of the $J-V$ data had been collected, meaning that the mini-modules had already been exposed to air and experienced thermal stress for quite some time before SPO measurements. This explains why the efficiencies extracted from quasi-SPOs are not as high as those from the $J-V$ measurements.

3. CONCLUSIONS

In summary, we demonstrate successful blade coating and RTP for the fabrication of planar p−i−n PVSCs in an ambient environment. Both small devices and mini-modules have been made, with active areas of 0.105 and 2.7 cm^2, respectively. The best small device shows an average PCE of over 18.47% from forward and reverse scans, while the champion mini-module exhibits an average PCE of over 17.73% from scans of different directions. In addition, these efficiencies are accompanied by high fill factors, with average values of 79.90 and 74.77% for the best small device and mini-module, respectively. The efficiency of our top mini-module is the highest so far for square centimeter-scale PVSCs annealed by RTP. Furthermore, the RTP method reduces the annealing time of blade-coated $MAPbI_3$ films from 2 min for hot plate to less than 30 s. This 4-fold decrease of annealing time will facilitate the road toward high-speed coating of perovskite layers. These results validate the practicability of using the RTP method for upscaling the manufacturing of PVSCs. Likely, blade coating will be replaced by slot-die coating to realize R2R printing and large-scale manufacturing of PVSCs.

4. MATERIALS AND METHODS

4.1. Chemicals. Poly(triaryl amine) (PTAA) was purchased from Sigma-Aldrich. Lead iodide (PbI_2, 99.9985%) and methylammonium iodide (MAI) were acquired from Alfa Aesar and Greatcell Solar, respectively. Methylammonium chloride (MACl, >98.0%) and bathocuproine (BCP, >99.0%, sublimed) were obtained from TCI. Poly[(9,9-bis(3′-(*N*,*N*-dimethylamino)propyl)-2,7-fluorene)-*alt*-2,7-(9,9-dioctylfluorene)] dibromide (PFN-Br) was ordered from 1-Material. Fullerene C60 (>99.5%) was purchased from Lumtec. All solvents, such as toluene, methanol, *N*,*N*-dimethylformamide (DMF), dimethyl sulfoxide (DMSO), and *N*-methyl-2-pyrrolidone (NMP), were purchased from Sigma-Aldrich in anhydrous grade.

4.2. Device Fabrication. The ITO glass were cut into slides of 1 inch in width and 5 inch in length, which were ultrasonically brushed with Liquinox detergent solution (Liquinox/DI water = 1:20), and then rinsed with DI water thoroughly. After N_2 blow-drying, the cleaned ITO-glass slide substrates were treated by the UV−ozone for 15 min and then used immediately for sequential coating of different layers. All of the blade coating, hot-plate annealing, and RTP were performed in an ambient environment. Regardless of solution type, 20 μL of solution was applied for a substrate with a dimension of 1 × 5 $inch^2$. PTAA was dissolved in toluene to form a 10 mg/mL solution. PTAA layer was blade-coated with a gap height of ∼100 μm at a coating speed of 10 mm/s and then annealed at 100 °C for 10 min. After the PTAA layer, PFN in methanol (0.4 mg/mL) was employed to modify the hydrophobicity of PTAA.[43] PFN was blade-coated with the same coating parameters but no annealing. On top of the PFN layer, the perovskite layer was blade-coated with a gap height of ∼150 μm at a coating speed of 7.5 mm/s. Perovskite precursor solution was composed of 1.2 M MAI, 1.2 M PbI_2, and 0.06 M MACl in a mixed solvent (DMF/DMSO/NMP = 0.91:0.07:0.02 volume ratio). The coating recipe was adopted from ref 5, in which the thickness has been optimized for this specific recipe. No antisolvent was used. Instead, an air-knife was employed to predry the blade-coated perovskite films before annealing of any kind. The gas quenching was utilized before both the hot-plate annealing and RTP annealing. The gas quenching is used to extract the solvent and dry the wet films, aiming at promoting nucleation[44] and formation of a supersaturated intermediate state.[45,46] The as-deposited films were transparent before the quenching, after which they turned a specular brownish color. The ITO-glass slides were further cut into 1 × 1 $inch^2$ substrates. For the control sets, perovskite films were annealed at 140 °C for 2 min on a hot plate. For the RTP samples, different RTP conditions were utilized as outlined in Table S1. The RTP instrument was a commercial Ulvac MILA-3000 minilamp annealer. The thermocouple inside the RTP instrument is attached to a piece of silicon. Samples were floating above the silicon piece without any physical contact, meaning that the measured temperature was not necessarily the same as the actual temperature of the sample. After annealing, the 1 × 1 $inch^2$ substrates were loaded into a thermal evaporator for consecutive deposition of C_{60}, BCP, and silver, with thicknesses of 30, 6, and 100 nm, respectively.

https://dx.doi.org/10.1021/acsaem.0c00180
ACS Appl. Energy Mater. 2020, 3, 3714−3720

4.3. Characterization. The X-ray diffraction (XRD) data were measured by a Bruker D8 Discover X-ray diffractometer. UV−vis spectrophotometer (Cary 6000-i) was used to collect the absorption spectra. The top-view SEM images were recorded using a JEOL 7000 field-emission scanning electron microscope (SEM). The $J-V$ curves were measured by a Class AAA solar simulator with a Xe-arc lamp and AM1.5G filter from PV measurement, and illumination intensity was calibrated with an NREL-certified Si reference cell. A monochromator (Newport 74100) and optical power meter (Newport 70310) were utilized to measure the external quantum efficiency (EQE) with a xenon lamp (Newport 66902) and a Si detector (Newport 71640).

■ ASSOCIATED CONTENT

Supporting Information

The Supporting Information is available free of charge at https://pubs.acs.org/doi/10.1021/acsaem.0c00180.

Optimization process of RTP versus hot-plate annealing (Table S1); trends of (a) efficiency, (b) FF, (c) J_{sc}, and (d) V_{oc} at different RTP temperatures for 5, 10, and 20 s (Figure S1); box charts of (a) efficiency, (b) FF, (c) J_{sc}, and (d) V_{oc} for mini-modules annealed by RTP and hot plate (Figure S2) (PDF)

■ AUTHOR INFORMATION

Corresponding Authors

Dawen Li − *Department of Electrical and Computer Engineering, Center for Materials for Information Technology, The University of Alabama, Tuscaloosa, Alabama 35487, United States;* orcid.org/0000-0001-8991-5431; Email: dawenl@eng.ua.edu

Maikel F. A. M. van Hest − *National Renewable Energy Laboratory, Golden, Colorado 80401, United States;* Email: Maikel.van.Hest@nrel.gov

Authors

Zhongliang Ouyang − *Department of Electrical and Computer Engineering, Center for Materials for Information Technology, The University of Alabama, Tuscaloosa, Alabama 35487, United States*

Mengjin Yang − *National Renewable Energy Laboratory, Golden, Colorado 80401, United States*

James B. Whitaker − *National Renewable Energy Laboratory, Golden, Colorado 80401, United States*

Complete contact information is available at: https://pubs.acs.org/10.1021/acsaem.0c00180

Notes

The authors declare no competing financial interest.

■ ACKNOWLEDGMENTS

This work is partially supported by the National Science Foundation (NSF) (No. 1753822). D.L. acknowledges graduate student scholarship for Z.O. from the Center for Materials for Information Technology (MINT) at the University of Alabama. This work was supported by the Alliance for Sustainable Energy, LLC, the manager and operator of the National Renewable Energy Laboratory for the U.S. Department of Energy (DOE) under Contract No. DE-AC36-08GO28308. The views expressed in the article do not necessarily represent the views of the DOE or the U.S. Government. The U.S. Government retains, and the publisher, by accepting the article for publication, acknowledges that the U.S. Government retains a nonexclusive, paid-up, irrevocable, worldwide license to publish or reproduce the published form of this work, or allow others to do so, for U.S. Government purposes.

■ REFERENCES

(1) Kojima, A.; Teshima, K.; Shirai, Y.; Miyasaka, T. Organometal Halide Perovskites as Visible-Light Sensitizers for Photovoltaic Cells. *J. Am. Chem. Soc.* **2009**, *131*, 6050−6051.

(2) Yang, Y.; You, J. Make Perovskite Solar Cells Stable. *Nature* **2017**, *544*, 155−156.

(3) Rong, Y.; Hu, Y.; Mei, A.; Tan, H.; Saidaminov, M. I.; Seok, S. I.; McGehee, M. D.; Sargent, E. H.; Han, H. Challenges for Commercializing Perovskite Solar Cells. *Science* **2018**, *361*, No. eaat8235.

(4) Wang, Y.; Dar, M. I.; Ono, L. K.; Zhang, T.; Kan, M.; Li, Y.; Zhang, L.; Wang, X.; Yang, Y.; Gao, X.; et al. Thermodynamically Stabilized β-CsPbI3−based Perovskite Solar Cells with Efficiencies >18%. *Science* **2019**, *365*, 591−595.

(5) Yang, M.; Li, Z.; Reese, M. O.; Reid, O. G.; Kim, D. H.; Siol, S.; Klein, T. R.; Yan, Y.; Berry, J. J.; van Hest, M. F.; Zhu, K. Perovskite Ink with Wide Processing Window for Scalable High-efficiency Solar Cells. *Nat. Energy* **2017**, *2*, No. 17038.

(6) Zhong, Y.; Munir, R.; Li, J.; Tang, M.-C.; Niazi, M. R.; Smilgies, D.-M.; Zhao, K.; Amassian, A. Blade-coated Hybrid Perovskite Solar Cells with Efficiency >17%: An In Situ Investigation. *ACS Energy Lett.* **2018**, *3*, 1078−1085.

(7) Li, C.; Yin, J.; Chen, R.; Lv, X.; Feng, X.; Wu, Y.; Cao, J. Monoammonium Porphyrin for Blade-Coating Stable Large-Area Perovskite Solar Cells with >18% Efficiency. *J. Am. Chem. Soc.* **2019**, *141*, 6345−6351.

(8) Li, Z.; Klein, T. R.; Kim, D. H.; Yang, M.; Berry, J. J.; van Hest, M. F.; Zhu, K. Scalable Fabrication of Perovskite Solar Cells. *Nat. Rev. Mater.* **2018**, *3*, No. 18017.

(9) Cheng, P.; Bai, H.; Zawacka, N. K.; Andersen, T. R.; Liu, W.; Bundgaard, E.; Jørgensen, M.; Chen, H.; Krebs, F. C.; Zhan, X. Roll-Coated Fabrication of Fullerene-Free Organic Solar Cells with Improved Stability. *Adv. Sci.* **2015**, *2*, No. 1500096.

(10) Schmidt, T. M.; Larsen-Olsen, T. T.; Carle, J. E.; Angmo, D.; Krebs, F. C. Upscaling of Perovskite Solar Cells: Fully Ambient Roll Processing of Flexible Perovskite Solar Cells with Printed Back Electrodes. *Adv. Energy Mater.* **2015**, *5*, No. 1500569.

(11) Kim, D. H.; Whitaker, J. B.; Li, Z.; van Hest, M. F.; Zhu, K. Outlook and Challenges of Perovskite Solar Cells Toward Terawatt-scale Photovoltaic Module Technology. *Joule* **2018**, *2*, 1437−1451.

(12) Im, J.-H.; Jang, I.-H.; Pellet, N.; Graetzel, M.; Park, N.-G. Growth of CH3NH3PbI3 Cuboids with Controlled Size for High-efficiency Perovskite Solar Cells. *Nat. Nanotechnol.* **2014**, *9*, 927−932.

(13) Ahn, N.; Son, D.-Y.; Jang, I.-H.; Kang, S. M.; Choi, M.; Park, N.-G. Highly Reproducible Perovskite Polar Cells with Average Efficiency of 18.3% and Best Efficiency of 19.7% Fabricated via Lewis Base Adduct of Lead (II) Iodide. *J. Am. Chem. Soc.* **2015**, *137*, 8696−8699.

(14) Bi, C.; Wang, Q.; Shao, Y.; Yuan, Y.; Xiao, Z.; Huang, J. Non-Wetting Surface-driven High-aspect-ratio Crystalline Grain Growth for Efficient Hybrid Perovskite Solar Cells. *Nat. Commun.* **2015**, *6*, No. 7747.

(15) You, J.; Meng, L.; Song, T.-B.; Guo, T.-F.; Yang, Y. M.; Chang, W.-H.; Hong, Z.; Chen, H.; Zhou, H.; Chen, Q.; Liu, Y.; De Marco, N.; Yang, Y. Improved Air Stability of Perovskite Solar Cells via Solution-processed Metal Oxide Transport Layers. *Nat. Nanotechnol.* **2016**, *11*, 75−81.

(16) Chiang, C.-H.; Wu, C.-G. Bulk Heterojunction Perovskite−PCBM Solar Cells with High Fill Factor. *Nat. Photonics* **2016**, *10*, 196−200.

(17) Koushik, D.; Verhees, W. J.; Kuang, Y.; Veenstra, S.; Zhang, D.; Verheijen, M. A.; Creatore, M.; Schropp, R. E. High-efficiency Humidity-stable Planar Perovskite Solar Cells Based on Atomic Layer Architecture. *Energy Environ. Sci.* **2017**, *10*, 91−100.

(18) Tan, H.; Jain, A.; Voznyy, O.; Lan, X.; de Arquer, F. P. G.; Fan, J. Z.; Quintero-Bermudez, R.; Yuan, M.; Zhang, B.; Zhao, Y.; et al. Efficient and Stable Solution-processed Planar Perovskite Solar Cells via Contact Passivation. *Science* **2017**, *355*, 722−726.
(19) Yang, W. S.; Park, B.-W.; Jung, E. H.; Jeon, N. J.; Kim, Y. C.; Lee, D. U.; Shin, S. S.; Seo, J.; Kim, E. K.; Noh, J. H.; Seok, S. I. Iodide Management in Formamidinium-lead-halide−based Perovskite Layers for Efficient Solar Cells. *Science* **2017**, *356*, 1376−1379.
(20) Arora, N.; Dar, M. I.; Hinderhofer, A.; Pellet, N.; Schreiber, F.; Zakeeruddin, S. M.; Grätzel, M. Perovskite Solar Cells with CuSCN Hole Extraction Layers Yield Stabilized Efficiencies Greater than 20%. *Science* **2017**, *358*, 768−771.
(21) Turren-Cruz, S.-H.; Saliba, M.; Mayer, M. T.; Juárez-Santiesteban, H.; Mathew, X.; Nienhaus, L.; Tress, W.; Erodici, M. P.; Sher, M.-J.; Bawendi, M. G.; et al. Enhanced Charge Carrier Mobility and Lifetime Suppress Hysteresis and Improve Efficiency in Planar Perovskite Solar Cells. *Energy Environ. Sci.* **2018**, *11*, 78−86.
(22) Luo, D.; Yang, W.; Wang, Z.; Sadhanala, A.; Hu, Q.; Su, R.; Shivanna, R.; Trindade, G. F.; Watts, J. F.; Xu, Z.; et al. Enhanced Photovoltage for Inverted Planar Heterojunction Perovskite Solar Cells. *Science* **2018**, *360*, 1442−1446.
(23) Xu, J.; Hu, Z.; Jia, X.; Huang, L.; Huang, X.; Wang, L.; Wang, P.; Zhang, H.; Zhang, J.; Zhang, J.; Zhu, Y. A Rapid Annealing Technique for Efficient Perovskite Solar Cells Fabricated in Air Condition under High Humidity. *Org. Electron.* **2016**, *34*, 84−90.
(24) Wang, K.-L.; Zhang, C.-C.; Jiang, Y.-R.; Liu, H.-R.; Li, X.-M.; Jain, S. M.; Ma, H. High-quality Perovskite Pilms via Post-annealing Microwave Treatment. *New J. Chem.* **2019**, *43*, 9338−9344.
(25) Cao, Q.; Yang, S.; Gao, Q.; Lei, L.; Yu, Y.; Shao, J.; Liu, Y. Fast and Controllable Crystallization of Perovskite Films by Microwave Irradiation Process. *ACS Appl. Mater. Interfaces* **2016**, *8*, 7854−7861.
(26) Jeon, T.; Jin, H. M.; Lee, S. H.; Lee, J. M.; Park, H. I.; Kim, M. K.; Lee, K. J.; Shin, B.; Kim, S. O. Laser Crystallization of Organic−inorganic Hybrid Perovskite Solar Cells. *ACS Nano* **2016**, *10*, 7907−7914.
(27) Li, F.; Zhu, W.; Bao, C.; Yu, T.; Wang, Y.; Zhou, X.; Zou, Z. Laser-assisted Crystallization of CH3NH3PbI3 Films for Efficient Perovskite Solar Cells with A High Open-circuit Voltage. *Chem. Commun.* **2016**, *52*, 5394−5397.
(28) Muydinov, R.; Seeger, S.; Kumar, S. H. B. V.; Klimm, C.; Kraehnert, R.; Wagner, M. R.; Szyszka, B. Crystallisation Behaviour of CH3NH3PbI3 Films: The Benefits of Sub-second Flash Lamp Annealing. *Thin Solid Films* **2018**, *653*, 204−214.
(29) Troughton, J.; Carnie, M. J.; Davies, M. L.; Charbonneau, C.; Jewell, E. H.; Worsley, D. A.; Watson, T. M. Photonic Flash-annealing of Lead Halide Perovskite Solar Cells in 1 ms. *J. Mater. Chem. A* **2016**, *4*, 3471−3476.
(30) Lavery, B. W.; Kumari, S.; Konermann, H.; Draper, G. L.; Spurgeon, J.; Druffel, T. Intense Pulsed Light Sintering of CH3NH3PbI3 Solar Cells. *ACS Appl. Mater. Interfaces* **2016**, *8*, 8419−8426.
(31) Ankireddy, K.; Ghahremani, A. H.; Martin, B.; Gupta, G.; Druffel, T. Rapid Thermal Annealing of CH3NH3PbI3 Perovskite Thin Films by Intense Pulsed Light with Aid of Diiodomethane Additive. *J. Mater. Chem. A* **2018**, *6*, 9378−9383.
(32) Ahmad, M. I.; Van Campen, D. G.; Fields, J. D.; Yu, J.; Pool, V. L.; Parilla, P. A.; Ginley, D. S.; Van Hest, M. F.; Toney, M. F. Rapid Thermal Processing Chamber for In-situ X-ray Diffraction. *Rev. Sci. Instrum.* **2015**, *86*, No. 013902.
(33) Sanchez, S.; Christoph, N.; Grobety, B.; Phung, N.; Steiner, U.; Saliba, M.; Abate, A. Efficient and Stable Inorganic Perovskite Solar Cells Manufactured by Pulsed Flash Infrared Annealing. *Adv. Energy Mater.* **2018**, *8*, No. 1802060.
(34) Pool, V. L.; Dou, B.; Van Campen, D. G.; Klein-Stockert, T. R.; Barnes, F. S.; Shaheen, S. E.; Ahmad, M. I.; Van Hest, M. F.; Toney, M. F. Thermal Engineering of FAPbI3 Perovskite Material via Radiative Thermal Annealing and In Situ XRD. *Nat. Commun.* **2017**, *8*, No. 14075.
(35) Park, J.; Choi, J. W.; Kim, W.; Lee, R.; Woo, H. C.; Shin, J.; Kim, H.; Son, Y. J.; Jo, J. Y.; Lee, H.; et al. Improvement of Perovskite Crystallinity by Omnidirectional Heat Transfer via Radiative Thermal Annealing. *RSC Adv.* **2019**, *9*, 14868−14875.
(36) Dou, B.; Pool, V. L.; Toney, M. F.; van Hest, M. F. Radiative Thermal Annealing/In Situ X-ray Diffraction Study of Methylammonium Lead Triiodide: Effect of Antisolvent, Humidity, Annealing Temperature Profile, and Film Substrates. *Chem. Mater.* **2017**, *29*, 5931−5941.
(37) Sanchez, S.; Hua, X.; Phung, N.; Steiner, U.; Abate, A. Flash Infrared Annealing for Antisolvent-Free Highly Efficient Perovskite Solar Cells. *Adv. Energy Mater.* **2018**, *8*, No. 1702915.
(38) Sánchez, S.; Vallés-Pelarda, M.; Alberola-Borràs, J.-A.; Vidal, R.; Jerónimo-Rendón, J. J.; Saliba, M.; Boix, P. P.; Mora-Seró, I. Flash Infrared Annealing As A Cost-effective and Low Environmental Impact Processing Method for Planar Perovskite Solar Cells. *Mater. Today* **2019**, *31*, 39−46.
(39) Bruening, K.; Dou, B.; Simonaitis, J.; Lin, Y.-Y.; van Hest, M. F.; Tassone, C. J. Scalable Fabrication of Perovskite Solar Cells to Meet Climate Targets. *Joule* **2018**, *2*, 2464−2476.
(40) Ouyang, Z.; Abrams, H.; Bergstone, R.; Li, Q.; Zhu, F.; Li, D. Rapid Layer-Specific Annealing Enabled by Ultraviolet LED with Estimation of Crystallization Energy for High-Performance Perovskite Solar Cells. *Adv. Energy Mater.* **2019**, *10*, No. 2070014.
(41) Deng, Y.; Van Brackle, C. H.; Dai, X.; Zhao, J.; Chen, B.; Huang, J. Tailoring Solvent Coordination for High-speed, Room-temperature Blading of Perovskite Photovoltaic Films. *Sci. Adv.* **2019**, *5*, No. eaax7537.
(42) Yang, M.; Kim, D. H.; Klein, T. R.; Li, Z.; Reese, M. O.; Tremolet de Villers, B. J.; Berry, J. J.; van Hest, M. F.; Zhu, K. Highly Efficient Perovskite Solar Modules by Scalable Fabrication and Interconnection Optimization. *ACS Energy Lett.* **2018**, *3*, 322−328.
(43) Lee, J.; Kang, H.; Kim, G.; Back, H.; Kim, J.; Hong, S.; Park, B.; Lee, E.; Lee, K. Achieving Large-area Planar Perovskite Solar Cells by Introducing An Interfacial Compatibilizer. *Adv. Mater.* **2017**, *29*, No. 1606363.
(44) Huang, F.; Li, M.; Siffalovic, P.; Cao, G.; Tian, J. From Scalable Solution Fabrication of Perovskite Films Towards Commercialization of Solar Cells. *Energy Environ. Sci.* **2019**, *12*, 518−549.
(45) Babayigit, A.; D'Haen, J.; Boyen, H.-G.; Conings, B. Gas Quenching for Perovskite Thin Film Deposition. *Joule* **2018**, *2*, 1205−1209.
(46) Brinkmann, K. O.; He, J.; Schubert, F.; Malerczyk, J.; Kreusel, C.; van gen Hassend, F.; Weber, S.; Song, J.; Qu, J.; Riedl, T. Extremely Robust Gas-Quenching Deposition of Halide Perovskites on Top of Hydrophobic Hole Transport Materials for Inverted (p−i−n) Solar Cells by Targeting the Precursor Wetting Issue. *ACS Appl. Mater. Interfaces* **2019**, *11*, 40172−40179.

https://dx.doi.org/10.1021/acsaem.0c00180
ACS Appl. Energy Mater. 2020, 3, 3714−3720